View metadata, citation and similar papers at core.ac.uk
brought to you by CORE
provided by Apollo

Discrete dislocation plasticity analysis of the high-temperature cyclic response of composites

Siamak S. Shishvan[a,b], Robert M. McMeeking[c,d], Tresa M. Pollock[e], Vikram S. Deshpande[b,*]

[a] *Department of Structural Engineering, University of Tabriz, P.O. Box 51666-16471, Tabriz, Iran*
[b] *Department of Engineering, University of Cambridge, Trumpington Street, Cambridge CB2 1PZ, UK*
[c] *Department of Materials and Department of Mechanical Engineering, University of California Santa Barbara, CA 93106, USA*
[d] *School of Engineering, University of Aberdeen, King's College, Aberdeen AB24 3UE, UK*
[e] *Department of Materials, University of California Santa Barbara, CA 93106-5050, USA*

Abstract

Discrete dislocation plasticity (DDP) analysis of the high-temperature cyclic deformation of two-phase composites comprising a plastic matrix and elastic precipitates is presented. Deformation of the matrix is by climb-assisted glide of dislocations while the precipitates deform by a combination of bulk elasticity and stress-driven interfacial diffusion. The DDP calculations predict a cyclically softening response due to the formation of dislocation cell structures within the matrix. The dislocation cell sizes decrease with decreasing size of the unit cell (or equivalently matrix channels) and this results in an increased cyclic softening rate in composites with smaller unit cells. Interfacial diffusion also enhances the formation of dislocation cell structures and thereby promotes cyclic softening. These results are consistent with predictions of the creep behaviour that indicate that the increase in the creep rate (i.e. tertiary creep) is also associated with the formation of dislocation cell structures within the matrix.

Keywords: High-temperature composite, cyclic loading, interfacial diffusion, discrete dislocation plasticity, size effects

1. Introduction

Nickel-based superalloys typically consist of a γ plastic matrix strengthened by over 50 vol.% of γ' elastic precipitates. These composites often exhibit stress softening during low cycle fatigue (LCF) at temperatures above $\sim 700^{\circ}$C [1, 2, 3]. This softening has been qualitatively associated with two critical micro-structural changes [4, 5]: (i) formation of

*Corresponding author
Email address: vsd@eng.cam.ac.uk (Vikram S. Deshpande)

dislocation networks in the γ phase and (ii) coarsening of the γ' precipitates. During prolonged cycling, dislocations rearrange and react with each other to form networks comprising primarily of edge dislocations. Concurrent with the formation of these dislocation structures in the γ phase, the γ' precipitates often coarsen at an accelerated rate. This coarsening is thought to be due to enhanced diffusional transport at the γ/γ' interfaces and postulated to be the cause of cyclic stress softening in high-temperature LCF [6]. The central goal of this study is to investigate via discrete dislocation plasticity (DDP) calculations the roles of interfacial diffusion and dislocation cell structure formation in the cyclic softening of two phase composites representative of nickel-based superalloys.

The low-temperature strength (i.e. when deformation is governed by the glide motion of dislocations) of such composites has been extensively investigated via DDP and is well known to be size dependent [7]; i.e. for a given volume fraction of elastic precipitates the strength increases with decreasing size of the unit cell (or equivalently the size of the precipitates). Modelling of the high-temperature behaviour of such composites has received less attention but recent advances in DDP modelling approaches for the high-temperature deformation of crystalline metals [8, 9] have aided such investigations. For example, Shishvan et al. [10] have extended the high-temperature DDP frameworks and developed a DDP approach to model the effect of stress-driven diffusion at the interfaces of multi-phase materials. Their study demonstrated that dislocation climb and interfacial diffusion reduce the effect of precipitate size on the high-temperature strength of such composites via the formation of low energy dislocation structures in the matrix phase. The same framework was then also used to demonstrate [11] that the formation of wavy γ/γ' interfaces in nickel-based superalloys triggers tertiary creep in these materials. The high-temperature DDP framework of Shishvan et al. [10] which explicitly models not only the climb of the dislocations but also stress-driven diffusion at the interfaces is ideally suited to test the various hypotheses for the mechanisms of stress softening during LCF. This is the focus of this study where we investigate the strain-controlled cyclic high-temperature response of composites akin to nickel-based superalloys.

The outline of the paper is as follows. We begin by briefly describing the DDP framework for modelling composites including the effects of interfacial diffusion as well as discussing the

material parameters used in the DDP calculations to represent the nickel-based superalloys. We then proceed to present DDP predictions with an emphasis on the mechanisms that govern the cyclically softening response of composites.

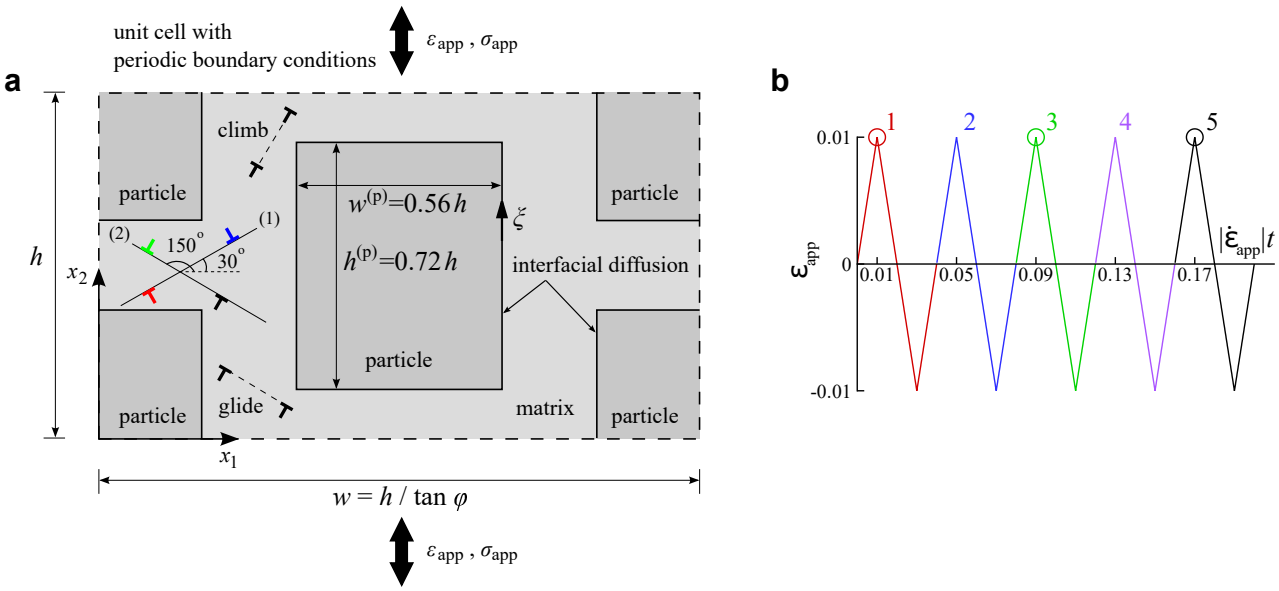

Figure 1: (a) Sketch of the unit cell of the composite subjected to uniaxial cyclic loading in the x_2 direction. The two active slip systems within the matrix are illustrated along with the positive and negative edge dislocations on these slip systems: the colours used to depict these dislocations are employed to illustrate dislocation structures in the remainder of the paper. (b) The applied cyclic strain history as a function of the normalised time $|\dot{\varepsilon}_{app}|\,t$. The circular symbols indicate the instants at which dislocation structures are plotted in Fig. 5.

2. DDP modelling of composites

We consider an infinitely large periodic composite with a brick and mortar microstructure and a unit cell of dimensions $w \times h$ as sketched in Fig. 1a. This composite comprising a percolated matrix and identical rectangular precipitates of dimensions $w^{(p)} \times h^{(p)}$ is subjected to uniaxial loading in the x_2 direction as sketched in Fig. 1a. Plane strain conditions are assumed to apply with deformation constrained in the $x_1 - x_2$ plane. Both the precipitates and the matrix are elastically isotropic with Young's modulus E and Poisson's

ratio ν. Deformation of the matrix phase is by a combination of glide and climb of edge dislocations (dislocation lines parallel to x_3) while the precipitates are assumed to undergo deformation by a combination of bulk elasticity and stress-driven interfacial diffusion at matrix/precipitate interfaces. Dislocation nucleation and motion within the matrix occurs on the slip systems oriented at angles $\varphi^{(1)} = \varphi = 30^{\rm o}$ and $\varphi^{(2)} = 180^{\rm o} - \varphi$ with respect to the x_1 axis (cf. Fig. 1a) and to ensure periodicity of the glide planes of the dislocations we set $w = h/\tan\varphi$. The composite has a volume fraction $V_{\rm f} \approx 46.6\%$ of precipitates and the aspect ratio of the precipitates was chosen to be $h^{(\rm p)}/w^{(\rm p)} = 9/7$ so as to ensure that the vertical and horizontal matrix channels are of approximately equal widths. We note in passing that dislocations cannot traverse the composite via pure glide without encountering in the impenetrable precipitates.

In DDP, the edge dislocations are treated as line defects with Burgers vector magnitude of b in an otherwise elastic continuum. Thus, plasticity is an outcome of the motion of these dislocations by a combination of glide and climb. While the long-range interactions of dislocations are captured by the linear elastic fields, the short-range interactions are incorporated through a set of constitutive rules [12, 13]. These constitutive rules are governed by the glide and climb components of the Peach-Koehler (P-K) force on each dislocation I denoted by $f_{\rm g}^{(I)}$ and $f_{\rm c}^{(I)}$, respectively. The glide velocity of dislocation I is defined by a linear drag relation $v_{\rm g}^{(I)} = f_{\rm g}^{(I)}/B_{\rm g}$ where $B_{\rm g}$ is the (glide) drag coefficient. Further, in line with previous investigations [13, 14, 15], we also assume a drag type relation for the climb velocity, i.e. $v_{\rm c}^{(I)} = f_{\rm c}^{(I)}/B_{\rm c}$ where the climb drag coefficient $B_{\rm c}$ is approximated from the Hirth and Lothe [16] estimate of the rate at which co-operatively climbing dislocations spaced a distance ℓ apart exchange vacancies. Following Danas and Deshpande [13], $B_{\rm c}$ at temperature T is specified as

$$B_{\rm c} = \frac{b^2 kT \ln(\ell/b)}{2\pi D_{\rm (v)} c_0 \Omega_{\rm (v)}^2}, \tag{1}$$

where $D_{\rm (v)}$ and c_0 are the vacancy diffusion coefficient and equilibrium vacancy concentration, respectively at temperature T, $\Omega_{\rm (v)}$ is the atomic vacancy volume and k the Boltzmann constant. Dislocation dipoles are nucleated from a density $\rho_{\rm nuc}$ of point Frank-Read sources

when the glide P-K force on these sources exceeds a magnitude $\tau_{\text{nuc}}b$ over a nucleation time t_{nuc}. Annihilation of two opposite signed dislocations on the same slip system occurs when they are within a material-dependent critical annihilation distance $L_{\text{e}} = 6b$. Point obstacles with a density ρ_{obs} are also randomly dispersed in the matrix with dislocations being unpinned from these obstacles when the glide P-K force on the dislocations exceeds $\tau_{\text{obs}}b$, where τ_{obs} is the obstacle strength.

Spatial gradients in the normal stress σ_{n} along the interface between the precipitate and matrix phases provide the driving force for diffusional mass transport (i.e. inter-diffusion of Al in Ni for nickel-based superalloys) along the interface. The interfacial mass transport is modelled as a normal velocity discontinuity across the interface specified by [17, 10]

$$\Delta v_{\text{n}} = -\frac{\partial}{\partial \xi}\left(\mathscr{D}_{(\text{i})}\frac{\partial \sigma_{\text{n}}(\xi)}{\partial \xi}\right), \tag{2}$$

where $\mathscr{D}_{(\text{i})}$ is the interfacial diffusion parameter and ξ is a local co-ordinate along the interface (Fig. 1a); see Shishvan et al. [10] for further details. Perfect bonding is assumed between the precipitates and the matrix so that there is no sliding across the interface and this DDP boundary value problem is solved using the superposition scheme described in [10].

DDP simulations typically require time-steps on the order of 0.5 ns to resolve short-range dislocation interactions. Thus, temporal scaling needs to be employed in order to perform simulations that are representative of experimental strain rates that are on the order $\dot{\varepsilon}^{\text{EXP}} \approx 10^{-7}$ s^{-1}. At these slow strain rates, vacancy diffusion driving dislocation climb and interfacial diffusion are the rate limiting deformation processes with dislocation glide occuring at a much faster rate. Following Shishvan et al. [11], we thus define two non-dimensional time scales: (i) the ratio of the vacancy diffusion to loading time-scale given by $\bar{\tau}_{(\text{v})} = \ell^2\dot{\varepsilon}^{\text{EXP}}/D_{(\text{v})}$ and (ii) the ratio of the interfacial diffusion to loading time-scale given by $\bar{\tau}_{(\text{i})} = \ell^3\dot{\varepsilon}^{\text{EXP}}/(\mathscr{D}_{(\text{i})}E)$. In order to ensure that the dominant deformation mechanisms in the scaled DDP calculations are the same as in the experiments, we require that both $\bar{\tau}_{(\text{v})}$ and $\bar{\tau}_{(\text{i})}$ are equal in the experiments and DDP calculations. Since we only implement a temporal scaling (i.e. no scaling of length scales and moduli), we use ℓ and E values in the simulations appropriate for composites representing nickel-based superalloys. Thus, the

scaling requirement reduces to $D^{\rm DDP}_{\rm (v)}/D^{\rm EXP}_{\rm (v)} = \dot{\varepsilon}^{\rm DDP}/\dot{\varepsilon}^{\rm EXP}$ and $\mathscr{D}^{\rm DDP}_{\rm (i)}/\mathscr{D}^{\rm EXP}_{\rm (i)} = \dot{\varepsilon}^{\rm DDP}/\dot{\varepsilon}^{\rm EXP}$, where the superscripts EXP and DDP denote the quantities in experiments on the composites and in the DDP simulations, respectively. Therefore, $\lambda \equiv \dot{\varepsilon}^{\rm DDP}/\dot{\varepsilon}^{\rm EXP}$ represents a speed-up factor in the DDP simulations compared to the experiments and the time t in the DDP calculations is related to time $t^{\rm EXP}$ in the experiments via $t^{\rm EXP} = \lambda t$.

2.1. Material parameters

The material parameters of the model are adapted from [10] and are representative of nickel-based superalloys. The elastic constants of the matrix and precipitates are $E = 100$ GPa and $\nu = 0.37$. The matrix is initially dislocation-free with a density $\rho_{\rm nuc} \simeq 300\mu{\rm m}^{-2}$ of dislocation sources and a density $\rho_{\rm obs} \simeq 600\mu{\rm m}^{-2}$ of obstacles. These sources and obstacles were equally distributed on both slip systems and randomly located on slip planes spaced a distance $100b$ apart. These densities were chosen so as to ensure that the matrix in the absence of precipitates has negligible strain hardening for the unit cell sizes considered in this study [18, 19, 10]. The strength of each source is selected from a Gaussian distribution with an average of $\bar{\tau}_{\rm nuc} = 50$ MPa and standard deviation of 1 MPa while all obstacles have a strength $\tau_{\rm obs} = 150$ MPa. The nucleation time for all sources is taken as $t_{\rm nuc} = 10$ ns. In order to account for the inevitable statistical effects in DDP calculations, we present results that are averages over three realisations of the dislocation source and obstacle distributions. Dislocations on both slip systems have a Burgers vector of magnitude $b = 0.25$ nm and the glide drag coefficient for dislocation motion is $B_{\rm g} = 10^{-4}$ Pa s. The climb drag coefficient $B_{\rm c}$ requires the specification of the vacancy parameters as discussed subsequently.

Calculations are reported for composites at a temperature $T \simeq 1000$ °C with strain-controlled cyclic loading carried out over applied strains between $\varepsilon_{\rm app} = -0.01$ and 0.01. The atomic vacancy volume and c_0 at $T = 1000$ °C for nickel-based superalloys are $\Omega_{\rm (v)} = 13.8 \times 10^{-12}$ $\mu{\rm m}^3$, $c_0 = 20 \times 10^6$ $\mu{\rm m}^{-3}$, respectively and we choose the representative dislocation spacing ℓ to equal the slip plane spacing, i.e. $\ell = 100b$. It now remains to specify $D_{\rm (v)}$ in Eq. (1). The calculations reported here were designed to represent cyclic experiments carried out at an applied strain rate $|\dot{\varepsilon}^{\rm EXP}| = 2 \times 10^{-7}$ s^{-1}. In order to make these calculations

numerically feasible, we choose a speed-up factor $\lambda = 10^{10}$ and thus the DDP calculations were carried out at $\dot{\varepsilon}_{\text{app}} = \dot{\varepsilon}^{\text{DDP}}$ with $|\dot{\varepsilon}^{\text{DDP}}| = 2000\ \text{s}^{-1}$. Consequently, we are also required to scale the vacancy diffusion constant by λ. The vacancy diffusion coefficient at $T \simeq 1000\ ^{\circ}\text{C}$ in nickel-based superalloy is $D_{(\text{v})} = D^{\text{EXP}}_{(\text{v})} = 2\times10^{-5}\ \mu\text{m}^2\text{s}^{-1}$ which implies a scaled diffusion constant $D^{\text{DDP}}_{(\text{v})} = 2 \times 10^{5}\ \ \mu\text{m}^2\text{s}^{-1}$. Substituting these values in Eq. (1) with $D_{(\text{v})}$ replaced by $D^{\text{DDP}}_{(\text{v})}$, we obtain $B_{\text{c}} = 1$ Pa s. Similarly, the interfacial diffusion constant which governs the inter-diffusion of Al in Ni at $T \simeq 1000\ ^{\circ}\text{C}$ is $\mathscr{D}^{\text{EXP}}_{(\text{i})} = 5 \times 10^{-7}\ \mu\text{m}^5\text{N}^{-1}\text{s}^{-1}$ [20, 11] and this constant is also scaled by λ. Following [11] we report the effect of interfacial diffusion in terms of the non-dimensional parameter

$$\overline{\mathscr{D}} = \frac{\mathscr{D}_{(\text{i})}\ E}{D_{(\text{v})}\ \ell}, \tag{3}$$

which specifies the ratio of the vacancy diffusion to interfacial diffusion time. Calculations are reported for four cases, viz. composites with unit cell sizes $h = 0.5\ \mu\text{m}$ and $h = 1\ \mu\text{m}$ with interfacial diffusion absent ($\overline{\mathscr{D}} = 0$) and the reference value of $\overline{\mathscr{D}} = 0.1$ that follows from the experimental inter-diffusion constant of $\mathscr{D}^{\text{EXP}}_{(\text{i})} = 5 \times 10^{-7}\ \mu\text{m}^5\text{N}^{-1}\text{s}^{-1}$.

3. Results and discussion

DDP predictions of the cyclic response (5 cycles) of the $h = 0.5\,\mu\text{m}$ and $1\,\mu\text{m}$ composites are included in Figs. 2a and 2b, respectively for $\overline{\mathscr{D}} = 0.1$. These predictions are presented in terms of the normalised stress $\bar{\sigma}_{\text{app}} \equiv \sigma_{\text{app}}/\bar{\tau}_{\text{nuc}}$ versus ε_{app}, where σ_{app} is the work-conjugate to ε_{app}. Over the five cycles investigated here, the degree of cyclic softening is higher for the smaller unit cell ($h = 0.5\,\mu\text{m}$) composite. To better quantify this softening, we define a peak stress $\bar{\sigma}_{\text{p}}$ as the average of $\bar{\sigma}_{\text{app}}$ over the applied strain levels $0.005 \leq \varepsilon_{\text{app}} \leq 0.01$ and predictions of these peak stresses are included in Fig. 3 as a function of the cycle number. Consistent with the well-established size effect [7, 10], the initial strength (i.e. $\bar{\sigma}_{\text{p}}$ at the first cycle) of the composite increases with decreasing unit cell size h due to an increase in the density of geometrically necessary dislocations. Moreover, as discussed in Shishvan et al. [10] the strength decreases as interfacial diffusion rate is increased from $\overline{\mathscr{D}} = 0$ to $\overline{\mathscr{D}} = 0.1$. However, unlike monotonic loading where smaller unit cell composite display greater strain

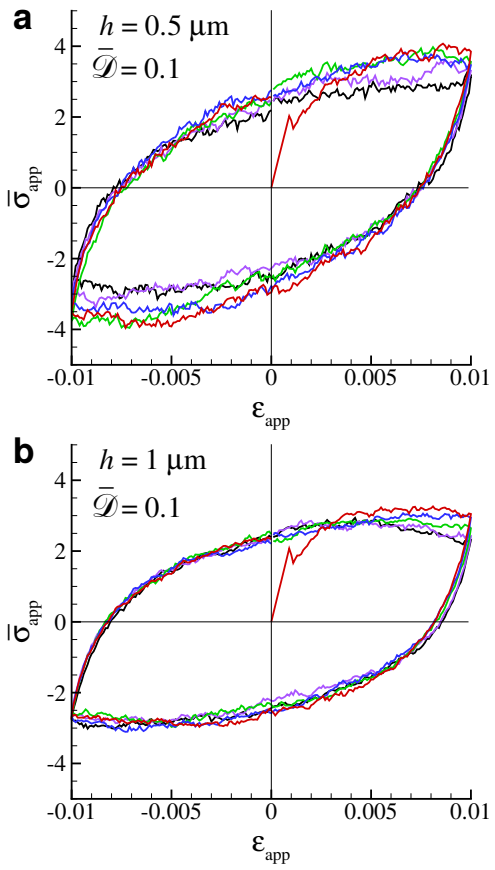

Figure 2: DDP predictions of the cyclic stress versus strain response for the (a) $h = 0.5\,\mu$m and (b) $h = 1\,\mu$m composites with $\overline{\mathscr{D}} = 0.1$.

hardening [10], the cyclic softening rate increases with decreasing h and this is especially evident in the $\overline{\mathscr{D}} = 0.1$ case. Thus, consistent with observations, the high-temperature DDP calculations predict a cyclic softening response and we proceed to understand the origins of this softening as well as its dependence on the unit cell size and interfacial diffusion.

Predictions of the evolution of the dislocation density ρ_{dis} within the matrix (i.e. the number of dislocations per unit matrix area) are plotted in Fig. 4a as a function of the normalised time $|\dot{\varepsilon}_{\text{app}}|t$. The fluctuations in the curves are a consequence of higher levels of nucleations during the tensile loading phase and increased annihilations of dislocations during the compressive loading phase. The overall dislocation density thus remains relatively stable for all except the $h = 0.5\,\mu$m composite with $\overline{\mathscr{D}} = 0.1$ in which case the dislocation

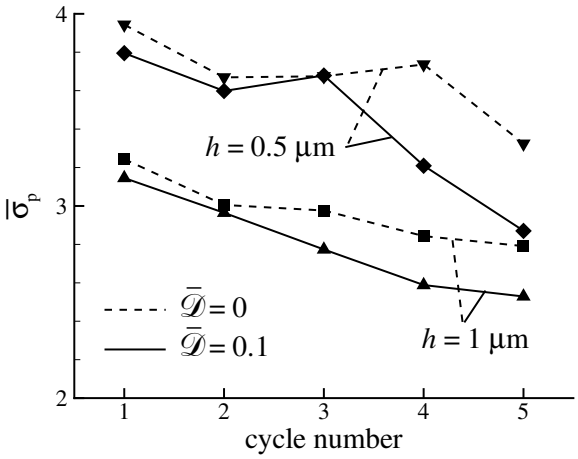

Figure 3: Predictions of the peak cyclic stress $\bar{\sigma}_{\rm p}$ as a function of the number of cycles (lines are drawn as a guide to the eye).

density increases with cycle number. To understand the effect of this increase in dislocation density on the deformation, we define average strain measures

$$\bar{\epsilon}_{\rm g} = \frac{1}{A^{(\rm m)}} \int_{A^{(\rm m)}} \sum_{\alpha=1}^{2} \left| s_i^{(\alpha)} E_{ij} m_j^{(\alpha)} \right| {\rm d}A, \tag{4}$$

and

$$\bar{\epsilon}_{\rm c} = \frac{1}{A^{(\rm m)}} \int_{A^{(\rm m)}} \sum_{\alpha=1}^{2} \left| m_i^{(\alpha)} E_{ij} m_j^{(\alpha)} \right| {\rm d}A, \tag{5}$$

to quantify the deformation within the matrix due to dislocation glide and climb, respectively. Here, $A^{(\rm m)}$ is the area of the matrix while $s_i^{(\alpha)}$ and $m_i^{(\alpha)}$ are unit vectors in the slip direction and normal to the slip plane in slip system (α), respectively. The strain estimates $E_{ij} = 0.5(u_{i,j} + u_{j,i})$ are calculated by numerically differentiating the total displacement field u_i using the FE mesh comprising square bi-linear elements of size 0.01 μm. Predictions of the temporal evolution of $\bar{\epsilon}_{\rm g}$ and $\bar{\epsilon}_{\rm c}$ are included in Figs. 4b and 4c, respectively, for all four cases analysed here. While both the glide and climb strains show an increasing trend in all cases, again a marked increase in the matrix strain rates is predicted for the $h = 0.5$ μm composite with $\overline{\mathscr{D}} = 0.1$, starting at approximately the third loading cycle.

The increase in the strain rates $\dot{\bar{\epsilon}}_{\rm g}$ and $\dot{\bar{\epsilon}}_{\rm c}$ seen in Figs. 4b and 4c is better understood by examining the dislocation structures in the $h = 0.5$ μm and $h = 1$ μm composites shown

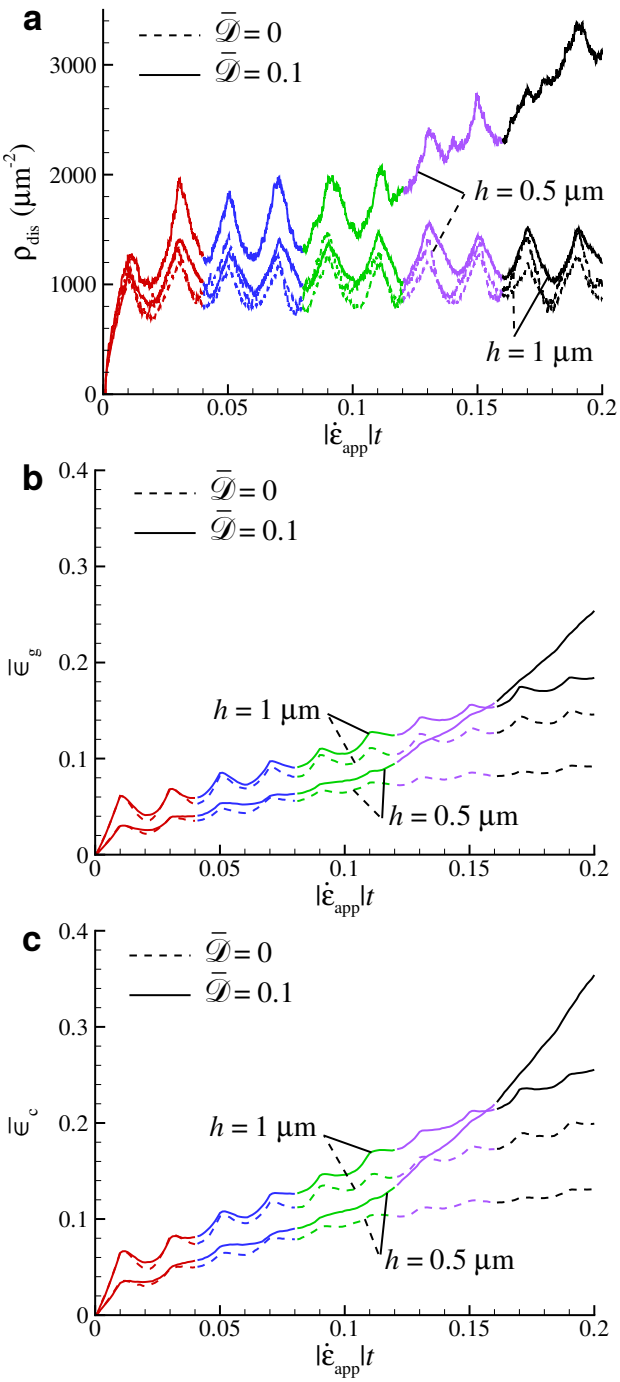

Figure 4: Temporal evolution of (a) dislocation density, (b) matrix strain due to dislocation glide and (c) matrix strain due to dislocation climb. These temporal evolutions are shown for all four cases investigated here as a function of the normalised time $|\dot{\varepsilon}_{\mathrm{app}}|\, t$. The colours of different parts of the curves indicate the cycle number using the colour coding indicated in Fig. 1b.

in Figs. 5a and 5b, respectively. The dislocation structures in Fig. 5 are shown at the peak strains in the first, third and fifth cycles (see Fig. 1b). The formation of dislocation cells commences at the third cycle and we argue that the increase in the strain rates $\dot{\bar{\epsilon}}_{\rm g}$ and $\dot{\bar{\epsilon}}_{\rm c}$ follow the formation of these cell structures. The dislocation arrays that form the cell walls are pathways for fast vacancy diffusion and thus in turn increases the dislocation climb rates. The higher dislocation climb rates then allow dislocations to circumvent the precipitates at a higher rate which enhances the glide rate of the dislocations and results in softening. The dislocation cell structures are constrained by the width of the matrix channels and thus smaller cells form in the $h = 0.5\,\mu$m composite. Therefore, the DDP calculations predict higher climb rates and increased cyclic softening in the $h = 0.5\,\mu$m composite compared to the $h = 1\,\mu$m composite. We emphasise that the dislocation cell structures predicted by the DDP calculations are consistent with a wide body of observations [4, 21, 22, 23] reported for high-temperature LCF of nickel-based superalloys.

Dislocation cell structures also form during the creep of nickel-based superalloys [11] and thus the role of load reversal in stress softening during high-temperature LCF has been the topic of numerous experimental investigations [24, 25]. We now proceed to use the DDP calculations to ascertain what role the reversal of the applied strain rates (i.e. cyclic loading) plays in the development of dislocation cell structures and begin by reporting predictions of the creep responses of the composite in the four cases considered here. The creep responses are presented for a constant normalised applied stress $\bar{\Sigma}_{\rm app} = 2.95$ and 2.75 for the $h = 0.5\mu$m and 1 μm composites, respectively. These applied stresses are approximately the average stresses during the tensile loading phase (i.e. $\bar{\Sigma}_{\rm app} \simeq \langle \bar{\sigma}_{\rm app} \rangle$ for $\dot{\varepsilon}_{\rm app} > 0$) of the cyclic response of these composites.

Predictions of the creep responses are included in Fig. 6 with the creep time defined as $t_{\rm cr} \equiv \lambda(t - t_{\rm R})$, where $t_{\rm R}$ is the time in the DDP calculations to ramp the applied stress to attain the constant value $\bar{\Sigma}_{\rm app}$ and λ the temporal scaling constant. Thus, $t_{\rm cr}$ is representative of experimental time-scales and the creep strain $\varepsilon_{\rm cr}$ is the accumulated strain over $t_{\rm cr} \geq 0$. The creep strain rates $\dot{\varepsilon}_{\rm cr}$ in Fig. 6 are high from early in the time history for the $h = 1\,\mu$m composite. On the other hand, the creep strain rates of the

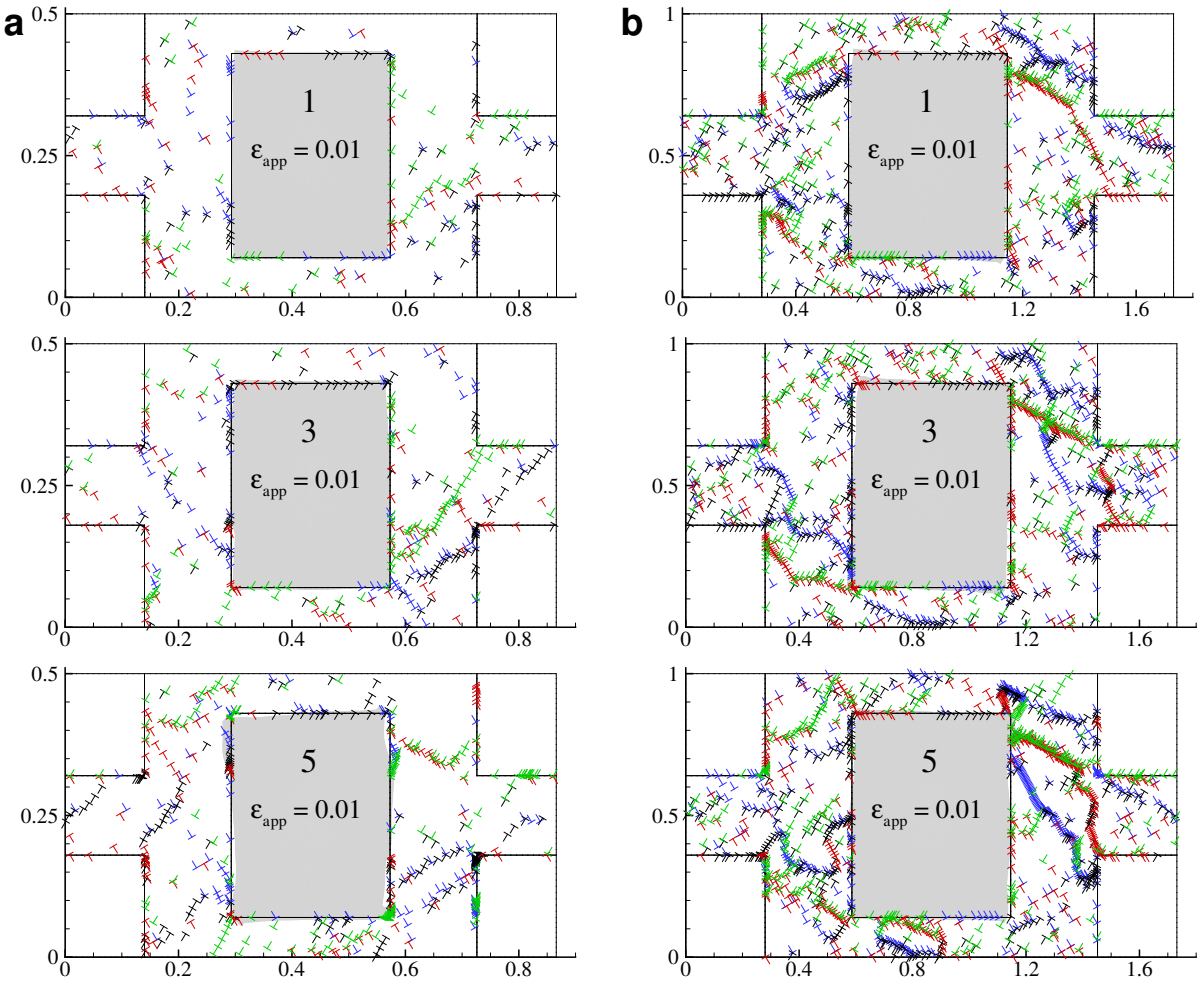

Figure 5: The evolution of the dislocation structures in the (a) $h = 0.5\ \mu$m and (b) $h = 1\ \mu$m composites ($\overline{\mathscr{D}} = 0.1$) during loading cycles 1, 3 and 5 as indicated by the circular markers in Fig. 1b. The deformation of the central precipitate is indicated in each case with the displacements magnified by a factor of 5 and 10 in (a) and (b), respectively. The colours assigned to dislocations are defined in Fig. 1a and all dimensions are in μm.

$h = 0.5\,\mu$m composite increase significantly around $t_{\rm cr} = 75$ hrs and 200 hrs for the $\overline{\mathscr{D}} = 0.1$ and $\overline{\mathscr{D}} = 0$ cases, respectively. To better understand these creep responses, we include in Figs. 7a and 7b the dislocation structures in the $h = 0.5\,\mu$m composite with $\overline{\mathscr{D}} = 0.1$ at $t_{\rm cr} = 0$ and 75 hrs, respectively. Dislocation cell structures are clearly seen to form at $t_{\rm cr} = 75$ hrs and the formation of these cell structures corresponds to the onset of high creep strain rates under creep loading. This is analogous to the cyclic loading case where also the formation of dislocation cell structures co-incides with the onset of stress softening. Now recall that the third loading cycle (when cyclic softening is seen to initiate) also commences at $t^{\rm EXP} \approx 100$ hrs and we thus hypothesise that it is the formation of dislocation cells that results in softening under both constant stress creep loading and strain-controlled cyclic loading; i.e. the cyclic softerning is not dependent on the reversal of applied loading. Rather, dislocation cells form given sufficient time for vacancy (and interfacial) diffusion and the reversal of loading in the cyclic calculations does not change the mechanism significantly at least over the five cycles computed here. This is in agreement with the findings in [25] where increasing dwell time in creep-fatigue tests decreases the life of superalloy.

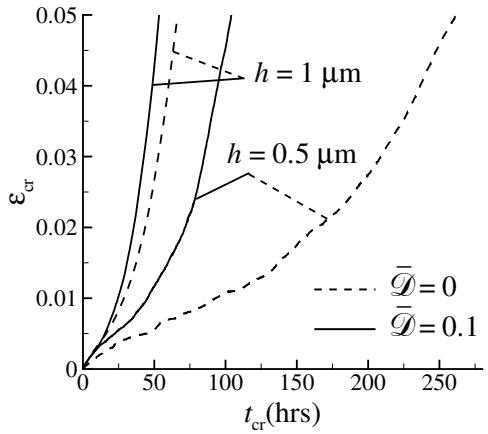

Figure 6: DDP predictions of the creep responses for normalised applied stresses $\bar{\Sigma}_{\rm app} \simeq 2.95$ and 2.75 for $h = 0.5\,\mu$m and $h = 1\,\mu$m composites, respectively.

Finally, it is worth discussing the role of interfacial diffusion. Interfacial diffusion is predicted to weaken the composites (increased softening under cyclic loading and higher

creep rates under creep loading). However, unlike continuum plasticity predictions [26], this weakening due to interfacial diffusion is not from enhanced large overall deformations of the precipitates. To illustrate this, we include in Figs. 5 and 7 the deformed shapes of the central precipitate. Clearly, the overall deformations of the precipitates are small. Instead interfacial diffusion promotes the formation of wavy interfaces between the matrix and the precipites with the amplitude of the waviness in the range $5b - 10b$ [11]. These local deformations of the interface relax the stresses within the matrix allowing for continued nucleation of dislocations. The continued nucleation of dislocations results in a high dislocation density (cf. Fig. 4a) with dislocation climb enabling the arrangement of these dislocations into low energy cell structures. Recall that these dislocation cell structures are the primary cause of softening of the composite and thus it follows that interfacial diffusion promotes softening.

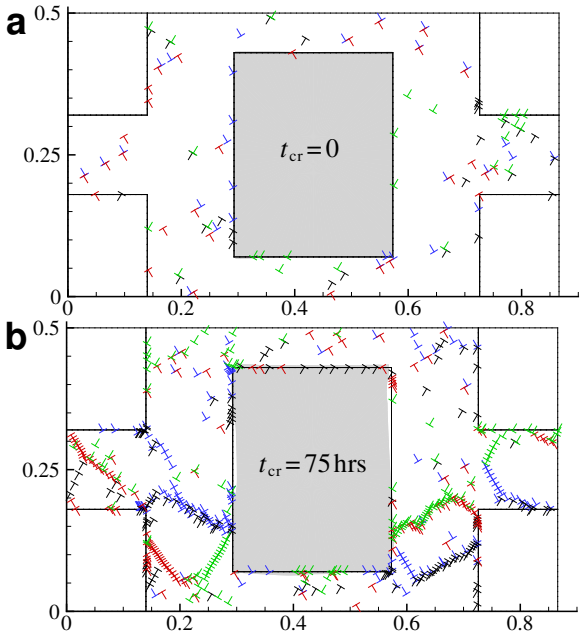

Figure 7: The evolution of the dislocation structure in the $h = 0.5\,\mu$m composite ($\overline{\mathscr{D}} = 0.1$) under a constant normalised applied stress $\bar{\Sigma}_{\text{app}} \simeq 2.95$ at times (a) $t_{\text{cr}} = 0$ and (b) $t_{\text{cr}} = 75$ hrs. The deformation of the central precipitate is indicated in each case with the displacements magnified by a factor of 5. The colours assigned to dislocations are defined in Fig. 1a and all dimensions are in μm.

4. Conclusions

DDP calculations are presented for the high-temperature strain-controlled cyclic loading of composites representative of nickel-based superalloys. The calculations confirm some existing hypotheses [5, 2] that cyclic softening is a result of formation of dislocation cell structures within the matrix phase. The formation of these cell structures is promoted by interfacial diffusion along the precipitate/matrix interfaces although, at least in the five cycles computed here, there was no coarsening of the precipitates due to global mass transport along the interfaces. Similar dislocation cell structures also formed under constant stress creep loading and therefore we hypothesise that the primary requirement for the formation of these dislocation structures is time to allow vacancy diffusion and associated dislocation climb rather than the load reversal that occurs during cyclic loading.

Acknowledgments

Support from ONR under grant numbers N62909-14-1N242 and N00014-14-1-0618 on Multi-scale methods for creep resistant alloys (program manager Dr. David Shifler) is gratefully acknowledged.

References

[1] T. P. Gabb, J. Gayda, R. V. Miner, Orientation and temperature dependence of some mechanical properties of the single-crystal nickel-base superalloy René N4: Part II. Low cycle fatigue behavior, Metall Mater Trans A 17 (1986) 497–505.

[2] T. P. Gabb, G. Welsch, The high temperature deformation in cyclic loading of a single crystal nickel-base superalloy, Acta Metall 37 (1989) 25072516.

[3] Z. He, Y. Zhang, W. Qiu, H. Shi, J. Gu, Temperature effect on the low cycle fatigue behavior of a directionally solidified nickel-base superalloy, Mater Sci Eng A 676.

[4] S. D. Antolovich, S. Liu, R. Baur, Low cycle fatigue behavior of René 80 at elevated temperature, Metall Mater Trans A 12 (1981) 473–481.

[5] S. D. Antolovich, E. Rosa, A. Pineau, Low cycle fatigue of René 77 at elevated temperatures, Mater Sci Eng 47 (1981) 47–57.

[6] C. Carry, J. L. Strudel, Apparent and effective creep parameters in single crystals of a nickel base superalloyI Incubation period, Acta Metall 25 (1977) 767–777.

[7] H. H. M. Cleveringa, E. Van der Giessen, A. Needleman, Comparison of discrete dislocation and continuum plasticity predictions for a composite material, Acta Mater 45 (1997) 3163–3179.

[8] C. Ayas, J. A. W. van Dommelen, V. S. Deshpande, Climb-enabled discrete dislocation plasticity, J Mech Phys Solids 62 (2014) 113–136.

[9] S. M. Keralavarma, A. A. Benzerga, High-temperature discrete dislocation plasticity, J Mech Phys Solids 82 (2015) 1–22.

[10] S. S. Shishvan, T. M. Pollock, R. M. McMeeking, V. S. Deshpande, Interfacial diffusion in high-temperature deformation of composites: a discrete dislocation plasticity investigation, J Mech Phys Solids 98 (2017) 330–349.

[11] S. S. Shishvan, R. M. McMeeking, T. M. Pollock, V. S. Deshpande, Discrete dislocation plasticity analysis of the effect of interfacial diffusion on the creep response of Ni single-crystal superalloys, Acta Mater 135 (2017) 188–200.

[12] E. Van der Giessen, A. Needleman, Discrete dislocation plasticity: a simple planar model, Modell Simul Mater Sci Eng 3 (1995) 689–735.

[13] K. Danas, V. S. Deshpande, Plane-strain discrete dislocation plasticity with climb-assisted glide motion of dislocations, Modell Simul Mater Sci Eng 21 (2013) 045008(26pp).

[14] D. Raabe, On the consideration of climb in discrete dislocation dynamics, Phil Mag A 77 (1998) 751–759.

[15] K. M. Davoudi, L. Nicola, J. J. Vlassak, Dislocation climb in two-dimensional discrete dislocation dynamics, J Appl Phys 111 (2012) 103522–1–7.

[16] J. P. Hirth, J. Lothe, Theory of Dislocations, Wiley, New York, 2 edn., 1982.

[17] A. Needleman, J. R. Rice, Plastic creep flow effects in the diffusive cavitation of grain boundaries, Acta Mettal 28 (1980) 1315–1332.

[18] M. I. Hussein, U. Borg, C. F. Niordson, V. S. Deshpande, Plasticity size effects in voided crystals, J Mech Phys Solids 56 (2008) 114–131.

[19] C. Ayas, L. C. P. Dautzenberg, M. G. D. Geers, V. S. Deshpande, Climb-enabled discrete dislocation plasticity analysis of the deformation of a particle reinforced composte, J Appl Mech 82 (2015) 071007–1–13.

[20] T. Ikeda, A. Almazouzi, H. Numakura, M. Koiwa, W. Sprengel, H. Nakajima, Single-phase interdiffusion in Ni_3Al, Acta Metall Mater 46 (1998) 5369–5376.

[21] J. H. Zhang, Z. Q. Hu, Y. B. Xu, Z. G. Wang, Dislocation structure in a single-crystal nickel-based

superalloy during low cycle fatigue, Metal Trans A 23A (1992) 1253–1258.

[22] V. Brien, B. Décamps, Low cycle fatigue of a nickel based superalloy at high temperature: deformation microstructures, Mater Sci Eng A 316 (2001) 18–31.

[23] X. G. Wang, J. L. Liu, T. Jin, X. F. Sun, Y. Z. Zhou, Z. Q. Hu, J. H. Do, B. G. Choi, I. S. Kimb, C. Y. Job, Deformation mechanisms of a nickel-based single-crystal superalloy during low-cycle fatigue at different temperatures, Scripta Mater 99 (2015) 57–60.

[24] Y. Jinjiang, S. Xiaofeng, J. Tao, Z. Nairen, G. Hengrong, H. Zhuangqi, High temperature creep and low cycle fatigue of a nickel-base superalloy, Mater Sci Eng A 527 (2010) 2379–2389.

[25] S. Duoqi, L. Jinlong, Y. Xiaoguang, Q. Hongyu, W. Jingke, Experimental investigation on low cycle fatigue and creep-fatigue interaction of DZ125 in different dwell time at elevated temperatures, Mater Sci Eng A 528 (2010) 233–238.

[26] P. Sofronis, R. M. McMeeking, The effect of interface diffusion and slip on the creep resistance of particulate composite materials, Mech Mater 18 (1994) 55–68.